The Solar System's Motion in the Galactic Tidal Field

Steve Wickson
215172
Physics 599
Final Report

Submitted to Dr. Phil Langill
January 19th, 2006

Abstract

The following pages will examine the solar system's dynamic interaction with its changing galactic environment as it orbits the center of the galaxy. Here we will attempt to quantify the effects that galactic tidal forces have on the Earth's orbit over millions of years using a series of models. Then we will discuss the limitations of the models we used and describe avenues for future research into the field of galaxy-solar system interactions.

Introduction

Presented is a rigorous mathematical analysis of the solar system's motion with respect to a varying local galactic tidal field strength. When immersed in a tidal field, a system of particles will separate and undergo tidal deformation. The space between the particles increases with the curvature of the gravitational potential. Recent observations of tidal tails on globular clusters near the galactic plane show that outer stars in the cluster are stripped off occasionally in the system's motion with respect to the galactic plane, 2006[6]. Using the Sun and the Earth as our objects of interest, the mechanism for galactic tidal perturbation can be illustrated with the following thought experiment:

Imagine the potential of our galaxy as being described by a curved funnel that takes the form of a hyperbolic or logarithmic function rotated about the vertical axis. Next we can imagine the Sun as a marble rolling around in this potential in a Rosette-shaped precessing elliptical orbit, typical of star orbits in spiral galaxies like the Milky Way[3]. Now imagine the Earth as a smaller marble that is attached to the Sun by a stretchable bond, keeping the planet attached to the Sun as it revolves around the center of the galaxy. When the Sun is at perigalacticon, the point in its orbit when it is closest to the galactic center, the slope of the potential is steepest and we should expect the spring to be more stretched than when the Sun is at apogalacticon, the point in its orbit when it is furthest from the galactic center. The stretch of the bond will contribute to an increase or decrease of the distance from the Earth to the Sun.

The illustration of the galactic tidal mechanism provided here merely helps to introduce the topic and does not claim to represent concrete, physical descriptions of these types of galaxy-solar system interactions. A more concrete attempt will be made in the following pages by first defining mathematical expressions for both the solar orbit and the gravitational potential of the Milky Way galaxy, and then deriving expressions for the components of the galaxy's tidal field. Using standard models of the Sun's orbit, the solar system's local galactic tidal field strength can be found as a function of time. Let us now begin our quest by first examining the solar system's motion in the galaxy.

The Sun's Orbit

The Sun is one of many millions of stars that orbit the galactic center. Detailed calculations show that star orbits in typical spiral galaxies like the Milky Way tend to trace out a rosette like shape when viewed from above[3]. The orbits of stars like the Sun also exhibit a form of vertical oscillation with respect to the plane of the galaxy's disk. Estimations for the orbital motion of the Sun are based on measurements of its galactocentric radius, R, its velocity with respect to other stars, and the galaxy's gravitational potential ,Φ, which will be described in greater detail in the next section.

The standard values for the Sun's galactocentric radius and circular velocity are $R_{\odot}$ = 8.5kpc and V_C = 220 kms^{-1}[1]. Based on these values, we can define the local standard of rest, which is an orbit defined by these two quantities to give a circular, planar approximation to the orbit of the Sun in the galaxy. However, in addition to the Sun's circular motion, it also moves with respect to the local standard of rest as a result of its oscillatory motion in the radial and vertical directions. The oscillatory motions of the Sun can be analysed in detail using epicycle approximations and tracing its position with respect to a circular, planar orbit. In fact, it is the Sun's motion relative to the local standard of rest that gives rise to the Rosette and Lissajous motions we see exhibited in Figures 2 and 3.

For the calculations in this report, we used a particular model for the solar orbit with the ordinary (R,θ,z) cylindrical coordinate system with the galactic center as the origin. Where R is the distance from the origin, in the direction parallel to the plane of the galaxy and z is the distance above or below the plane of the galactic disk. Most of the parameters for the solar system's motion were taken from the work of Frank Bash, 1986[1] and are summarized in the table below:

Table 1: Parameters for the Orbit of the Solar System, F.Bash, 1986[1]

$R_{\odot} = 8.5$ kpc	$e = 0.07$	$P_C = 237$ Myr
$z_{\odot} = +15$ pc	$R_{min} = 8.4575$ kpc	$P_R = 154$ Myr
$V_C = 220\ kms^{-1}$	$R_{max} = 9.7325$ kpc	$P_z = 66$ Myr
$V_R = -9\ kms^{-1}$	$z_{min} = -76.8$ pc	$t_{per} = +15$ Myr
$V_\theta = +12\ kms^{-1}$	$z_{max} = +76.8$ pc	$t_{gp} = -2.1$ Myr
$V_z = +7\ kms^{-1}$		

$R_{\odot}$ and $z_{\odot}$ are the coordinates for the Sun's position in the galaxy at present, V_C is the circular velocity and V_R, V_θ and V_z are the components of the Sun's velocity with respect to the local standard of rest. The Sun's orbit is given a value for the eccentricity, which we use to find the minimum and maximum values for the galactocentric radius, R_{min} and R_{max}. The vertical extremes, z_{min} and z_{max}, are the bounds of the Sun's vertical oscillation above and below the galactic plane. P_C and P_z are the circular and vertical oscillation periods respectively, and t_{per} and t_{gp} are the times of the closest perigalacticon passage and galactic plane crossings relative to the present. The Sun is currently approaching perigalaction, which Bash estimates this will occur 15 million years into the future. Also, according to Bash, the Sun passed through the galactic plane 2.1 million years ago and is moving in the +z direction towards its maximum height, which it will reach 14.6 million years into the future, near the same time it reaches perigalacticon.

The only value in the table that was not provided by Frank Bash is P_R, the anomalistic period of the Sun's orbit, which is defined as the period of time between two successive perigalacticon passages. This information was required in order to completely define the Sun's orbit and so a value of 154 million years was adopted, which is well within the range provided in Binney & Tremaine[3]. Using these parameters we can define the Sun's equations of motion in parametric form:

$$\begin{aligned} \theta(t) &= (2\pi / P_C)t = 2\pi t / 237 \\ R(t) &= \tfrac{1}{2}(R_{max} + R_{min}) - \tfrac{1}{2}(R_{max} - R_{min})\cos(2\pi(t - t_{per}) / P_R) \\ &= 9.095 - 0.6375\cos(2\pi(t - 15)/154) \\ z(t) &= +z_{max}\sin(2\pi(t - t_{gp}) / P_z) = 0.0768\sin(2\pi(t + 2.1)/66) \end{aligned} \qquad (1)$$

We can also rewrite the Sun's planar motion in polar coordinates by isolating t in $\theta(t)$ and substituting this into R(t):

$$R(\theta) = 9.095 - 0.6375\cos((237\theta - 30\pi)/154) \qquad (2)$$

Figures 2 and 3 provide a representation of the Sun's motion in the R,θ and R,z planes that are a little easier on the eyes, plotted using Mathematica. The first plot expresses the orbit that the Sun would trace out over the last 601 million years and up to the next perigalacticon passage, 15 million years into the future if viewed from a vantage point directly above the galaxy's plane. As expected, this forms a Rosette shape just like typical star orbits in galaxies.

```
ParametricPlot[{(9.095 - 0.6375 Cos[2 * Pi (t - 15) / 154]) Cos[ 2 * Pi * t / 237],
  (9.095 - 0.6375 Cos[2 * Pi (t - 15) / 154]) Sin [ 2 * Pi * t / 237]},
 {t, -601, 15}, AspectRatio → 1]
```

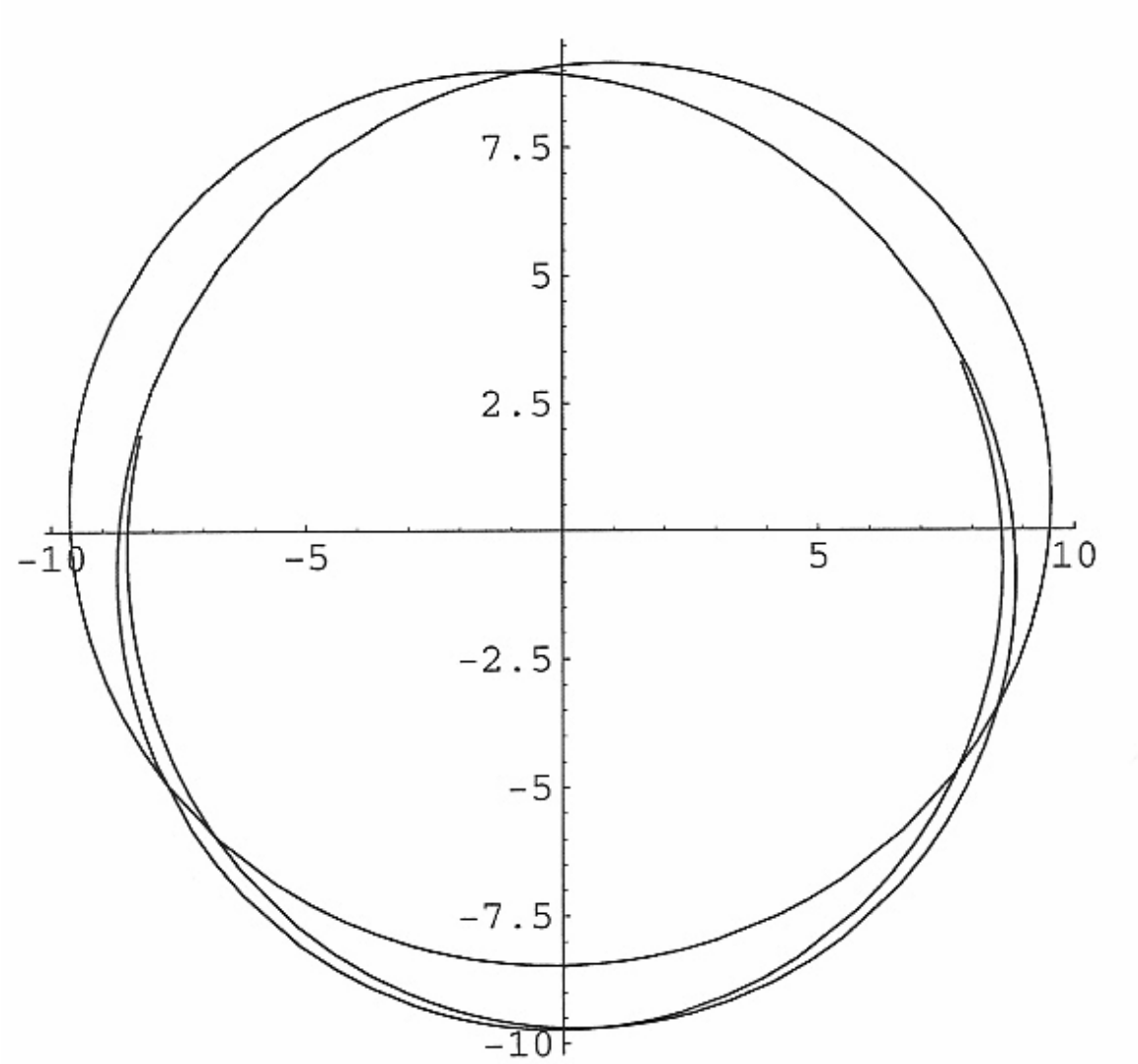

Figure 2: The Sun's orbital motion in the R,θ plane from 601 million years ago to 15 million years into the future, measured in kiloparsecs. The orbit traces out a Rosette shape around the origin, the galactic center.

The second plot is a representation of the Sun's motion with respect to a circular, planar orbit with the Sun's circular velocity of 220kms^{-1}. This is the typical path of a particle that is oscillating in two orthogonal directions at the same time, and thus represents the epicyclic motion of the Sun in the R and z directions.

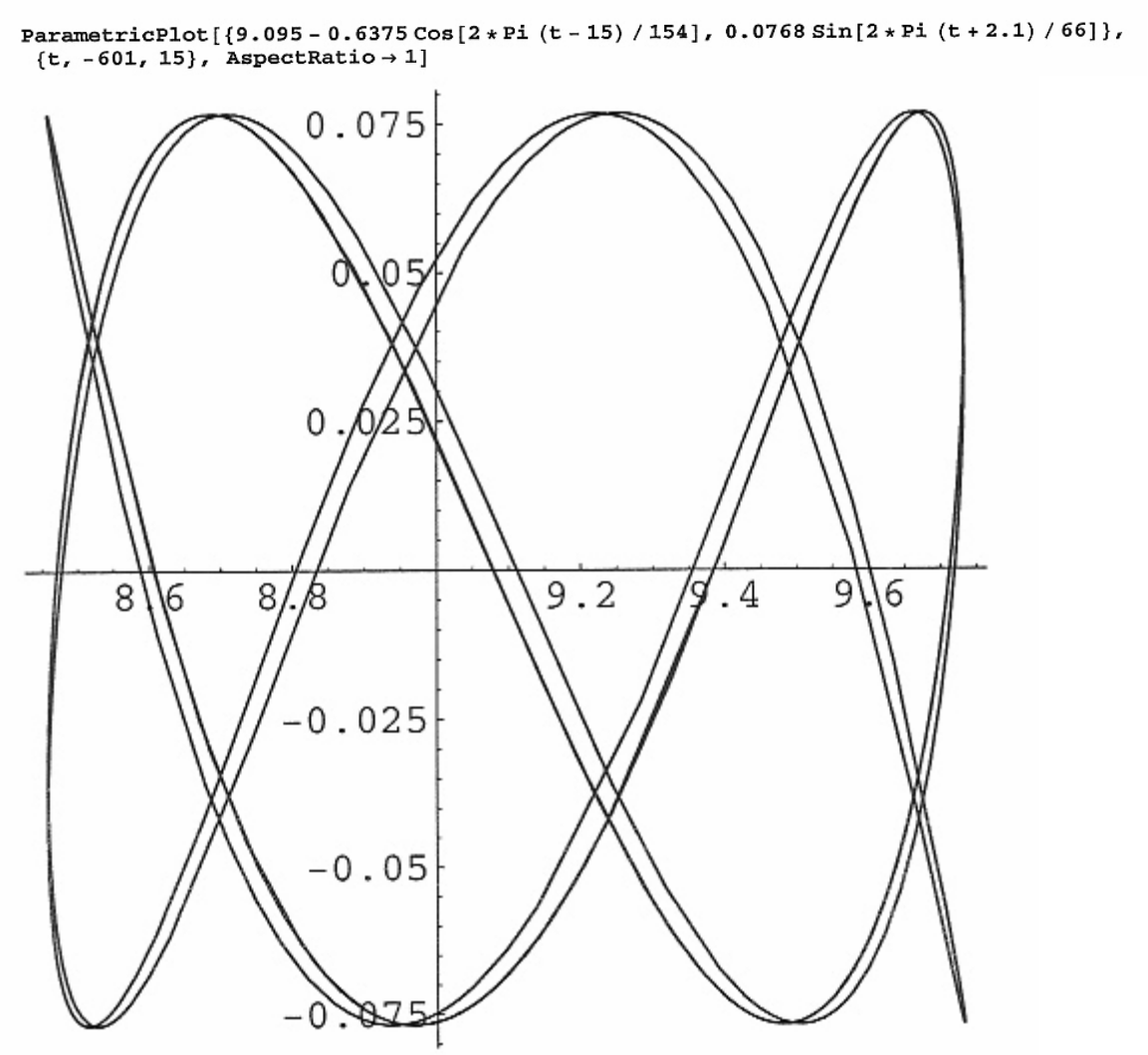

Figure 3: The Sun's orbit in the R,z plane from 601 million years ago to 15 million years into the future, measured in kiloparsecs. This represents the Sun's motion with respect to the Local Standard of Rest.

The Solar System's Orientation in the Galaxy

Before we go on to defining the galactic potential, it is worthwhile to calculate another important quantity that we will need later, the angle of inclination between the plane of the solar system and the galactic plane. We can do this by approximating the plane of the solar system as the ecliptic and measuring the angle between the North Galactic Pole (RA 12^h51^m, δ +27°7.7') = (192.86°, 27.13°)[2] and the North Ecliptic Pole (RA 18^h, δ +90-23°26.4') = (270°, 66.56)[16]. This is performed by using spherical

trigonometry to transfom the NGP into ecliptic coordinates and subtracting β, the ecliptic latitude from 90° (NEP).

$\sin \beta = \sin \delta \cos \varepsilon - \cos \delta \sin \alpha \sin \varepsilon$

$\beta = \arcsin[\sin 27.13° \cos 23.44° - \cos 27.13° \sin 192.86° \sin 23.44°]$

$= \underline{29.81°}, 150.19°$

Therefore, i, the angle of inclination between the ecliptic and galactic plane is

$90° - 29.81° = 60.21°$

This helps to write the components of the astronomical unit in galactic coordinates, as illustrated in Figure 4.

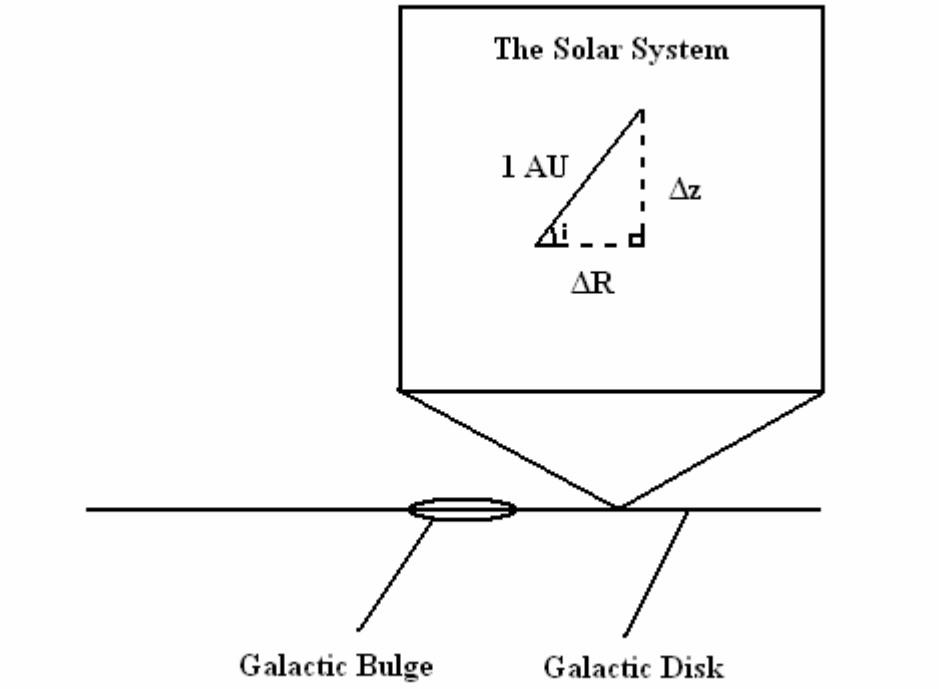

Figure 4: Components of the solar system plane in galactic coordinates.

The Galactic Potential

To make an estimation of the galactic tidal field, we need to begin by defining an expression for the gravitational potential of the Milky Way galaxy. The most reasonable estimates for the galactic potential are found from the collective position and velocity measurements of the visible stars and neutral hydrogen gas clouds in the galaxy. This can

provide us with a velocity-rotation diagram (Figure 5)[8], which is related to the gravitational potential by the simple equation

$$F_c = \frac{mV^2}{R} = -m\nabla\Phi = F_g \qquad (3)$$

which balances the centrifugal and gravitational forces, although this has the weakness of using circular orbit approximations. An expression for Φ can be found by rearranging the above equation and integrating. Φ can also be used to generate a density profile and total mass estimate for the galaxy via a combination of Poisson's equation and the divergence theorem:

$$4\pi GM = 4\pi G\iiint_V \rho d^3x = \iiint_V \nabla^2\Phi d^3x = \iint_S \nabla\Phi \cdot d^2S \qquad (4)$$

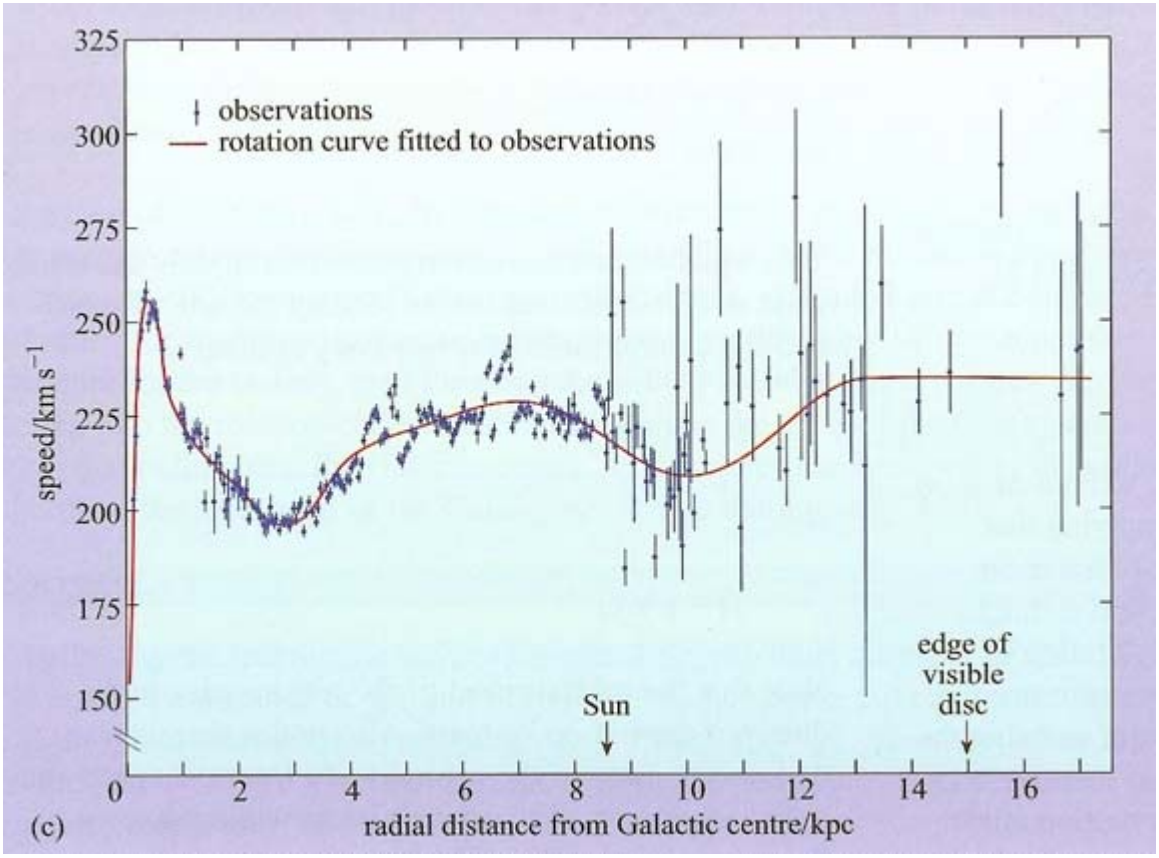

Figure 5: Velocity-Rotation diagram of the Milky Way, From Jones & Lambourne, 2004[8]. The data points represented in this figure are hydrogen gas cloud measurements.

Models for the gravitational potential of the galaxy are usually designed to fit both the observed velocity-rotation profiles and luminosity functions, as closely as possible. The galactic potential used in the following analysis is from a paper by Helmi & White, 2001[7].

Table 2: Components of the Galactic Potential, Helmi & White, 2001[7]

$$\Phi = \Phi_{Bulge} + \Phi_{Disk} + \Phi_{Halo}$$

$$\Phi(R,z) = -\frac{GM_{Bulge}}{c + \sqrt{R^2 + z^2}} - \frac{GM_{Disk}}{\sqrt{R^2 + (a + \sqrt{z^2 + b^2})^2}} + V_{Halo}^2 \ln(R^2 + z^2 + d^2)$$

Where the following constants are used,

Table 3: Parameters for the Galactic Potential, Helmi & White, 2001[7]

$M_{Bulge} = 3.4 \times 10^{10} M_{\odot}$	a = 6.5 kpc
$M_{Disk} = 10^{11} M_{\odot}$	b = 0.26 kpc
$V_{Halo} = 131.5 \text{ kms}^{-1}$	c = 0.7 kpc
	d = 12 kpc

Here, Φ is divided into three components. A pseudo-hyperbolic Hernqvist bulge component is used to model the central bulge region of the galaxy. The disk component of the galactic potential is modelled using one form of the standard Miyamoto-Nagai disk potential. Finally, a logarithmic halo component is added to more closely match the information given in velocity-rotation diagrams. The halo component is linked to the infamous dark matter problem that plagues current understanding of galactic astrophysics. The functions for the separate components of the potential are plotted in Figure 6.

The constants provided with the equation of Φ represent scale masses and scale heights for our particular model, although the halo component is scaled with a velocity squared parameter. This is one of the simplest analytic models for the galactic potential available, although I also performed calculations of the galactic tidal field using the 6 component potential given in Flynn, Sommer-Larsen & Christensen, 1996[5].

These expressions for Φ are only written as a function of R and z, thus neglecting θ dependent aspects of the galactic potential such as spiral arms. This merely reflects the fact that potential functions such as these are derived from velocity-rotation diagrams which use circular orbit approximations.

+0.1563 kpc^2Myr^{-2}

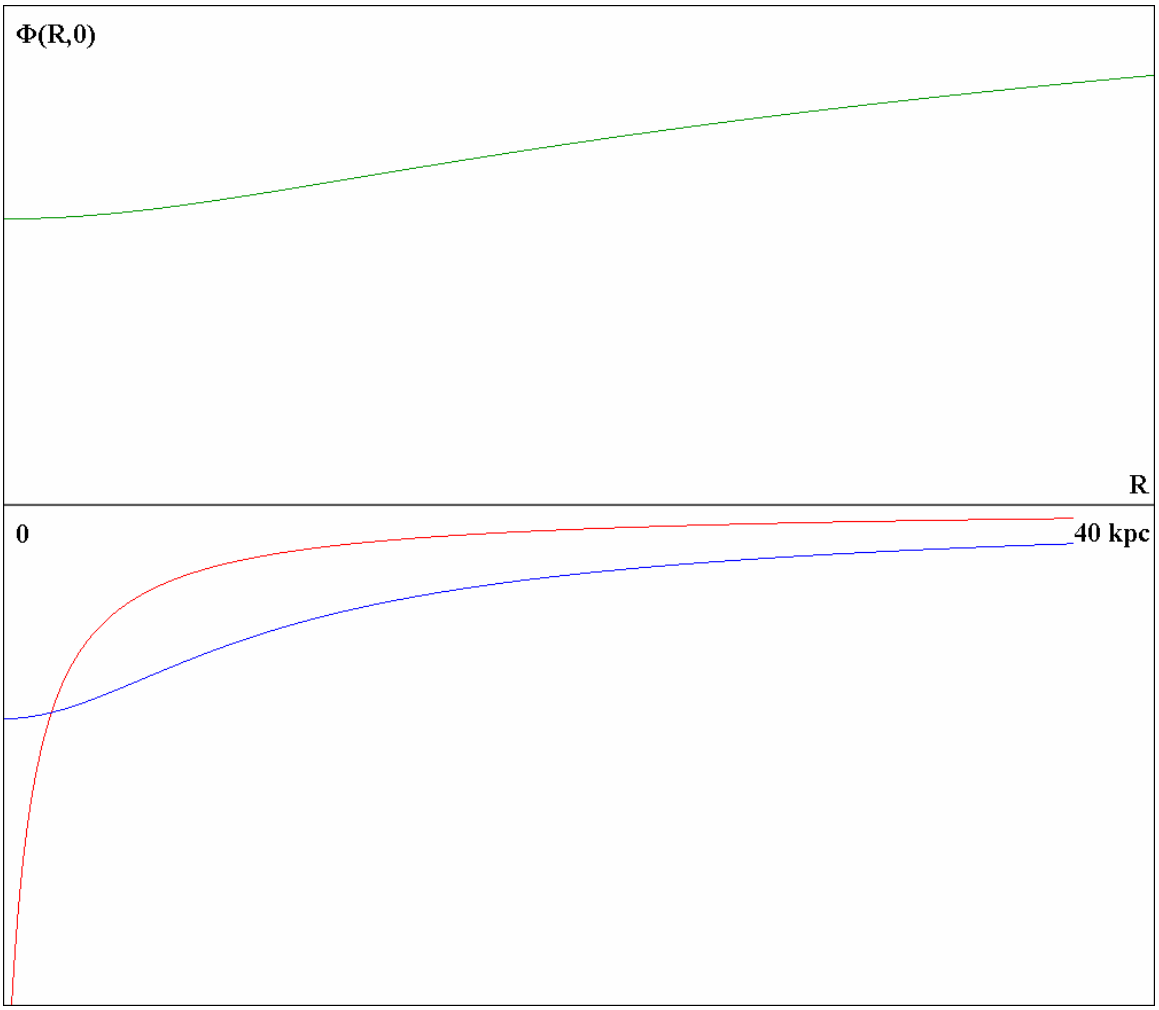

-0.1563 kpc^2Myr^{-2}

Figure 6: Bulge(red), Disk(blue) and Halo(green) components of the gravitational potential of the Milky Way in the central plane of the galaxy (z=0).

+0.1563 kpc^2Myr^{-2}

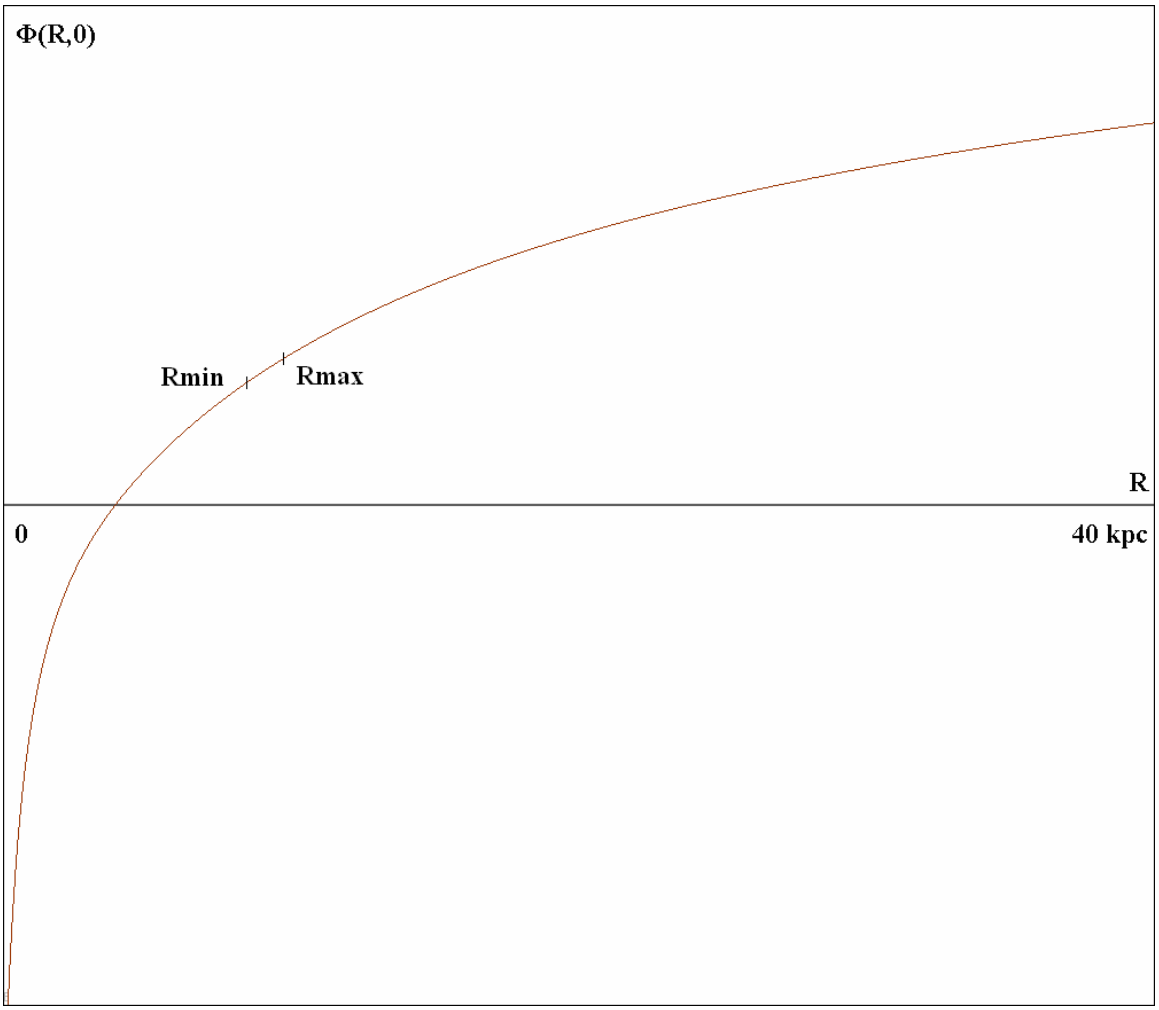

-0.1563 kpc^2Myr^{-2}

Figure 7: The total gravitational potential of the Milky Way as a function of R in the plane of the galaxy.

It is beneficial now to convert GM_{Bulge}, GM_{Disk} and V^2_{Halo} into units that are easier to work with, which will make the calculations a little easier. These quantities are converted into the elegant units of kpc^3Myr^{-2} in the following manner:

$$GM_{Bulge} = \frac{(3.4\times10^{10}\,M_{\odot})(1.327\times10^{11}\,km^3s^{-2}M_{\odot}^{-1})(3.156\times10^{13}\,sMyr^{-1})^2}{(3.086\times10^{16}\,kmkpc^{-1})^3}$$
$$= 0.153 kpc^3 Myr^{-2}$$
$$GM_{Disk} = \frac{(10^{11}\,M_{\odot})(1.327\times10^{11}\,km^3s^{-2}M_{\odot}^{-1})(3.156\times10^{13}\,sMyr^{-1})^2}{(3.086\times10^{16}\,kmkpc^{-1})^3} \quad (5)$$
$$= 0.450 kpc^3 Myr^{-2}$$
$$V_{Halo}^2 = \frac{(131.5 kms^{-1})^2(3.156\times10^{13}\,sMyr^{-1})^2}{(3.086\times10^{16}\,kmkpc^{-1})^2} = 0.018 kpc^2 Myr^{-2}$$

Written with these units, the galactic potential is plotted as a function of R, with z=0 in Figures 6 and 7. Figure 6 displays the relative contributions to the potential of the different components. Figure 7 shows the sum of all three components and so represents the total potential of the galaxy as a function of R. The Sun's minimum and maximum values of the galactocentric radius are also indicated on the plot to provide some reference to its location within the galactic potential.

Given a function for the scalar potential, we can find the gravitational field $\vec{F}$, which represents the gravitational force per unit mass. We find an expression for the gravitational field vector of the galaxy by taking the negative gradient of $\Phi(R,z)$:

$$\vec{F} = -\nabla\Phi(R,z) = -\frac{\partial\Phi}{\partial R}\hat{R} - \frac{\partial\Phi}{\partial z}\hat{z}$$

$$= \left[-\frac{GM_{Bulge}(R^2+z^2)^{-1/2}R}{(c+\sqrt{R^2+z^2})^2} - \frac{GM_{Disk}R}{(R^2+(a+\sqrt{z^2+b^2})^2)^{3/2}} - \frac{2V_{Halo}^2 R}{R^2+z^2+d^2}\right]\hat{R}$$
$$+\left[-\frac{GM_{Bulge}(R^2+z^2)^{-1/2}z}{(c+\sqrt{R^2+z^2})^2} - \frac{GM_{Disk}(a+\sqrt{z^2+b^2})(z^2+b^2)^{-1/2}z}{\sqrt{R^2+(a+\sqrt{z^2+b^2})^2}} - \frac{2V_{Halo}^2 z}{R^2+z^2+d^2}\right]\hat{z} \quad (6)$$

The gravitational field of the galaxy is plotted on the following pages, where the function in Figure 8 represents the gravitational field strength as a function of R, when z=0. This is scaled against the gravitational field strength as a function of z, where R=9.095, the mean galactocentric radius of the Sun's orbit, which is plotted below in Figure 9.

+0.1563 kpcMyr^{-2}

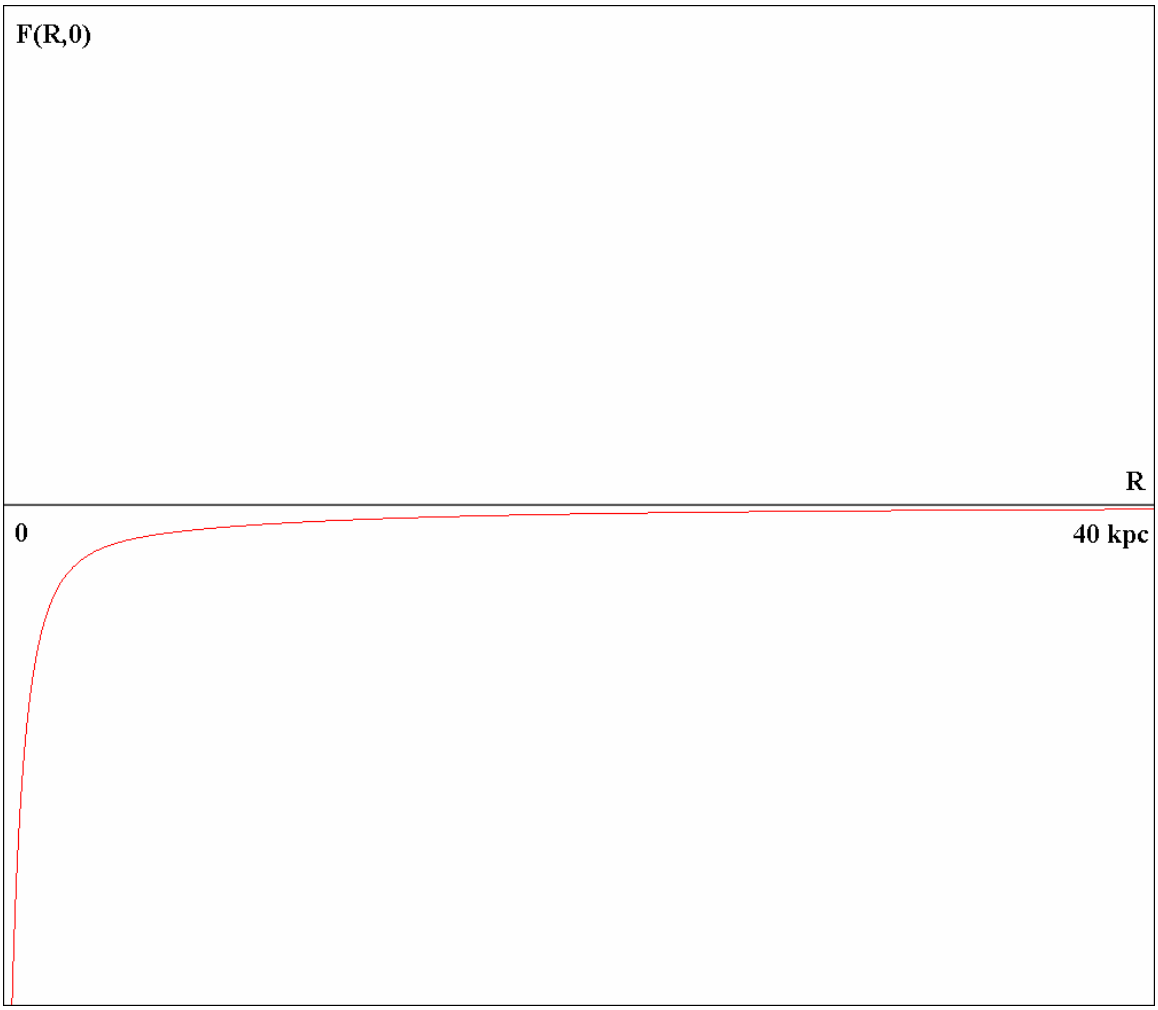

-0.1563 kpcMyr^{-2}

Figure 8: R component of the Galactic Gravitational Field as a function of R in the plane of the galaxy (z=0).

+0.1563 kpcMyr^{-2}

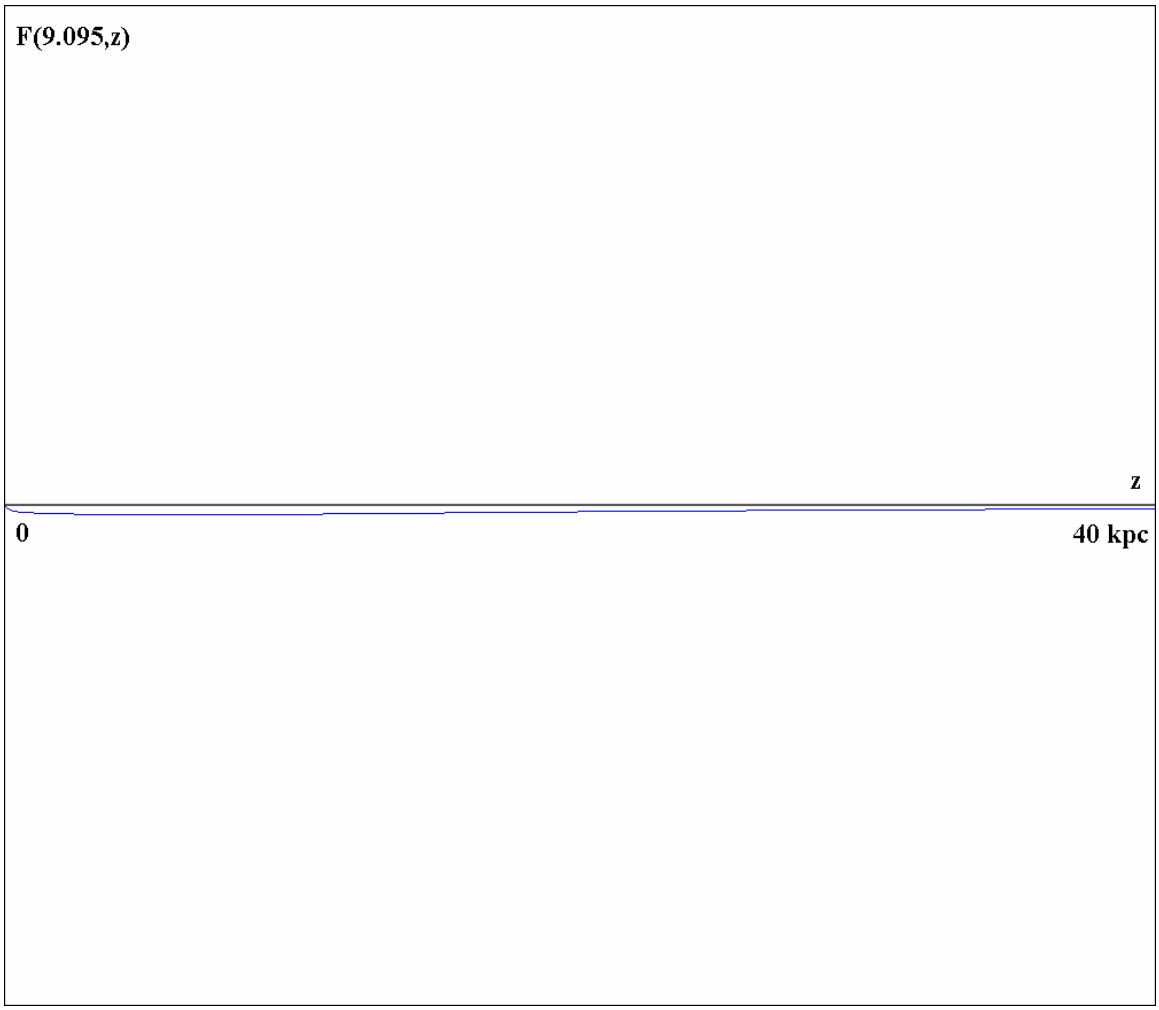

+0.1563 kpcMyr^{-2}

Figures 9: z component of the Galactic Gravitational Field with respect to the coordinates (9.095,z).

The Galactic Tidal Field

The tidal field of the Milky Way is then found by calculating the second partial derivatives of the gravitational potential with respect to R and z:

$$\frac{\partial^2\Phi}{\partial R^2} = \frac{GM_{Bulge}(1 + c(R^2+z^2)^{-1/2} - 3R^2(R^2+z^2)^{-1} - cR^2(R^2+z^2)^{-3/2})}{(c+\sqrt{R^2+z^2})^3}$$
$$+ \frac{GM_{Disk}(-2R^2 + (a+\sqrt{z^2+b^2})^2)}{(R^2+(a+\sqrt{z^2+b^2})^2)^{5/2}} + \frac{2V_{Halo}^2(-R^2+z^2+d^2)}{(R^2+z^2+d^2)^2}$$
$$\frac{\partial^2\Phi}{\partial R\partial z} = -\frac{GM_{Bulge}Rz((R^2+z^2)^{1/2} + c(R^2+z^2)^{-1/2} + 2(R^2+z^2)^{-1})}{(c+\sqrt{R^2+z^2})^3}$$
$$-\frac{3GM_{Disk}Rz(1+a(z^2+b^2)^{-1/2})}{(R^2+(a+\sqrt{z^2+b^2})^2)^{5/2}} - \frac{4V_{Halo}^2Rz}{(R^2+z^2+d^2)^2} = \frac{\partial^2\Phi}{\partial z\partial R}$$
$$\frac{\partial^2\Phi}{\partial z^2} = \frac{GM_{Bulge}(1 + c(R^2+z^2)^{-1/2} - 2z^2(R^2+z^2)^{-1} - cz^2(R^2+z^2)^{-3/2})}{(c+\sqrt{R^2+z^2})^3}$$
$$-\frac{3GM_{Disk}z^2(1+a(z^2+b^2)^{-1/2})^2}{(R^2+(a+\sqrt{z^2+b^2})^2)^{5/2}} + \frac{GM_{Disk}(1+a(z^2+b^2)^{-1/2} - az^2(z^2+b^2)^{-3/2})}{(R^2+(a+\sqrt{z^2+b^2})^2)^{3/2}}$$
$$+\frac{2V_{Halo}^2(R^2-z^2+d^2)}{(R^2+z^2+d^2)^2} \qquad (7)$$

These can be summarized in a 2×2 symmetric matrix, which we shall call $\overline{\overline{T}}$, the tidal force matrix. The Φ_{RR} and Φ_{zz} terms represent tidal stretching in R and z directions respectively. Φ_{Rz} terms mainly represent a shear or torsion in the tidal field, as explained by Dr. David Hobill at the University of Calgary[12]. $\overline{\overline{T}}$ can be used to find tidal accelerations

$$\delta a_x = -\frac{\partial \vec{F}_x}{\partial x}\Delta x \qquad (8)$$

by the operation

$$\begin{pmatrix}\delta a_R \\ \delta a_z\end{pmatrix} = \begin{pmatrix}\Phi_{RR} & \Phi_{Rz} \\ \Phi_{Rz} & \Phi_{zz}\end{pmatrix}\begin{pmatrix}\Delta R \\ \Delta z\end{pmatrix} \qquad (9)$$

δa_R and δa_z are the tidal accelerations in the R and z directions respectively, and ΔR and Δz are the components of a solar system orbit in galactic coordinates. In the case of the Earth's orbit

$$\Delta R = \cos i \times 1AU, \quad \Delta z = \sin i \times 1AU \qquad (10)$$

Modelling Galactic Tidal Field Variations

Now that we have a mathematical expression for the tidal field of the galaxy, we perform a series of calculations to model the effects of the galactic tides on the solar system as it moves through the galaxy over time. With each successive model, the situation becomes more realistic, but the mathematics more complex. Doing a simpler model first is a good place to start.

Model (I): The first model uses a hypothetical orbit that uses the Sun's equation of motion for R(t) but never leaves the plane of the galaxy (z=0 always), This annihilates the off diagonal terms of the tidal field matrix and makes it relatively easy to model the varying galactic tidal field strength as a function of time. So using the conditions z=0 and R(t)=9.095-0.6375cos(2π(t-15)/154) we plot $\Phi_{RR}(t)$ and $\Phi_{zz}(t)$ over the last 601 million years using Mathematica (Figures 10&11).

```
Plot[{-2 * 0.153 / (0.7 + (9.095 - 0.6375 Cos[2 * Pi (t - 15) / 154])) ^ 3 +
   0.450 ((6.5 + 0.26) ^ 2 - 2 (9.095 - 0.6375 Cos[2 * Pi (t - 15) / 154]) ^ 2) /
     ((6.5 + 0.26) ^ 2 + (9.095 - 0.6375 Cos[2 * Pi (t - 15) / 154]) ^ 2) ^ 2.5 +
   2 * 0.018 (12 ^ 2 - (9.095 - 0.6375 Cos[2 * Pi (t - 15) / 154]) ^ 2) /
     (12 ^ 2 + (9.095 - 0.6375 Cos[2 * Pi (t - 15) / 154]) ^ 2) ^ 2,
  - (5.7599 * 10 ^ -4) - (6.0774 * 10 ^ -5) Cos[2 * Pi (t - 15) / 154]}, {t, -601, 15}]
```

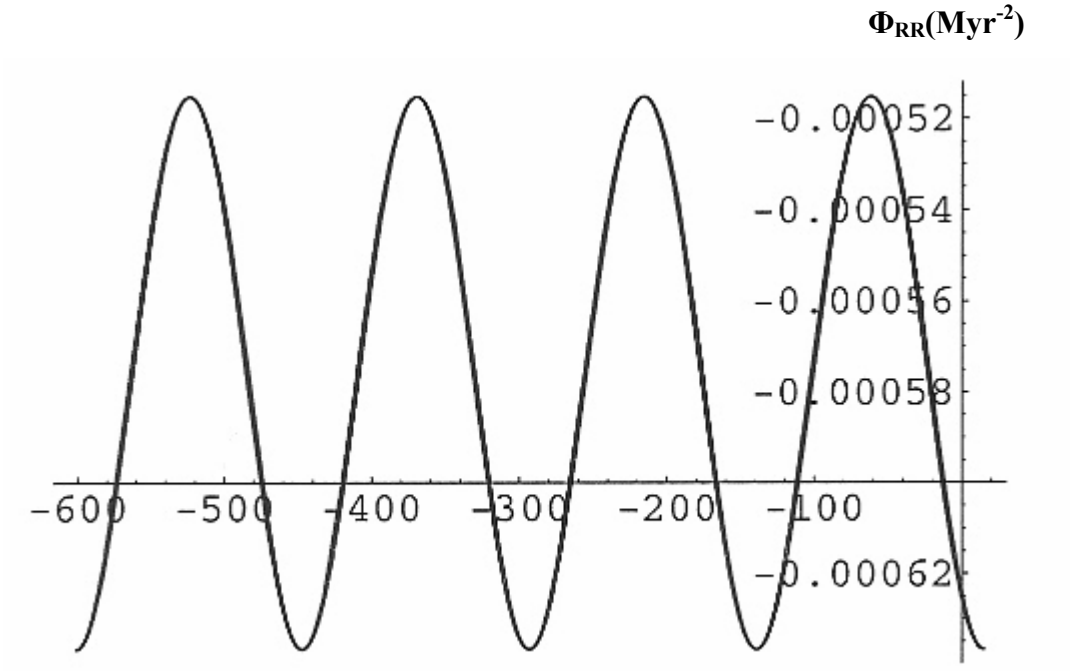

Figure 10: Φ_{RR} as a function of time over the last 601 million years, for our first model orbit of a star in the galactic plane.

```
Plot[{0.153 (1 + 0.7 / (9.095 - 0.6375 Cos[2 * Pi (t - 15) / 154])) /
      (0.7 + (9.095 - 0.6375 Cos[2 * Pi (t - 15) / 154])) ^ 3 +
    0.450 (1 + 6.5 / 0.26) / ((6.5 + 0.26) ^ 2 + (9.095 - 0.6375 Cos[2 * Pi (t - 15) / 154]) ^ 2) ^ 1.5 +
    2 * 0.018 (12 ^ 2 + (9.095 - 0.6375 Cos[2 * Pi (t - 15) / 154]) ^ 2) /
      (12 ^ 2 + (9.095 - 0.6375 Cos[2 * Pi (t - 15) / 154]) ^ 2) ^ 2,
  0.008463825 + 0.001137105 Cos[2 * Pi (t - 15) / 154]}, {t, -601, 15}]
```

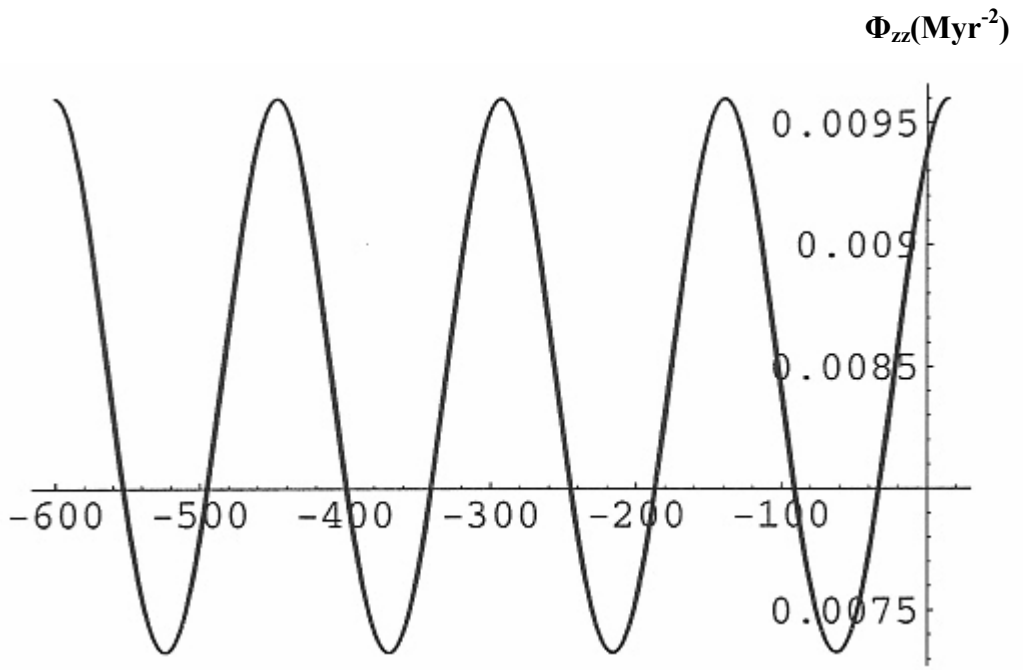

Figure 11: Φ_{zz} as a function of time over the last 601 million years, for our first model orbit of a star in the galactic plane.

The plots shown in Figures 10 & 11 display tidal field strength increasing and decreasing with the solar radial oscillation period of 154 million years. Also plotted on these graphs, on top of the original function, is a fit function, f(t). The fitting process involves evaluating the functions at the extrema and constructing a cosine function which approximates and simplifies the expression:

$$f(t) = \tfrac{1}{2}(\Phi_{RR\,max} + \Phi_{RR\,min}) + \tfrac{1}{2}(\Phi_{RR\,max} - \Phi_{RR\,min})\cos(2\pi(t - t_{min})/P_R) \qquad (11)$$

Often times the fit function matches the original, more complicated function so well, the plot looks like one curve. In subsequent calculations, the fit function will allow us to integrate more easily with respect to time. For the fit functions in the first model, we write:

$$\begin{aligned}
\Phi_{RR}(t) &= -5.76\times10^{-4}\,\mathrm{Myr}^{-2} - 6.08\times10^{-5}\,\mathrm{Myr}^{-2}\cos(2\pi(t-15\mathrm{Myr})/154\mathrm{Myr}) \\
\Phi_{Rz}(t) &= 0 \qquad (12) \\
\Phi_{zz}(t) &= 0.00846\mathrm{Myr}^{-2} + 0.00114\mathrm{Myr}^{-2}\cos(2\pi(t-15\mathrm{Myr})/154\mathrm{Myr})
\end{aligned}$$

Tidal accelerations can be found by:

$$\delta a_R(t) = \Phi_{RR}(t)\Delta R = \cos i\, \Phi_{RR}(t) \times 1\ \text{AU}$$
$$\delta a_z(t) = \Phi_{zz}(t)\Delta z = \sin i\, \Phi_{zz}(t) \times 1\ \text{AU} \qquad (13)$$

As shown in Figures 10&11, the $\delta a_z(t)$ function is about 33 times larger in amplitude and so the tidal forces are much stronger in the z direction than in the R direction. In this model, we can conclude that overall tidal acceleration is primarily due to the $\Phi_{zz}(t)$ function.

Model (II): Here we use a hypothetical orbit of a star that remains at the Sun's mean galactocentric radius of 9.095 kpc and undergoes vertical oscillations according to the Sun's equation for z(t). Substituting these conditions into the second partial derivatives of the potential, we get the plots seen in Figures 12,13&14.

```
R = 9.095; z = (0.0768 Sin[2 * Pi (t + 2.1) / 66]);

Plot[{0.153 (1 + 0.7 (R^2 + (0.0768 Sin[2 * Pi (t + 2.1) / 66]) ^2) ^-0.5 -
        3 R^2 (R^2 + (0.0768 Sin[2 * Pi (t + 2.1) / 66]) ^2) ^-1 -
        0.7 R^2 (R^2 + (0.0768 Sin[2 * Pi (t + 2.1) / 66]) ^2) ^-1.5) /
      (0.7 + (R^2 + (0.0768 Sin[2 * Pi (t + 2.1) / 66]) ^2) ^0.5) ^3 +
    0.450 (-2 R^2 + (6.5 + ((0.0768 Sin[2 * Pi (t + 2.1) / 66]) ^2 + 0.26^2) ^0.5) ^2) /
      (R^2 + (6.5 + ((0.0768 Sin[2 * Pi (t + 2.1) / 66]) ^2 + 0.26^2) ^0.5) ^2) ^2.5 +
    2 * 0.018 (-R^2 + (0.0768 Sin[2 * Pi (t + 2.1) / 66]) ^2 + 12^2) /
      (R^2 + (0.0768 Sin[2 * Pi (t + 2.1) / 66]) ^2 + 12^2) ^2,
   -(5.70399 * 10^-4) - (6.36 * 10^-7) Cos[2 * Pi (t + 2.1) / 33]}, {t,
   -139, 15}]
```

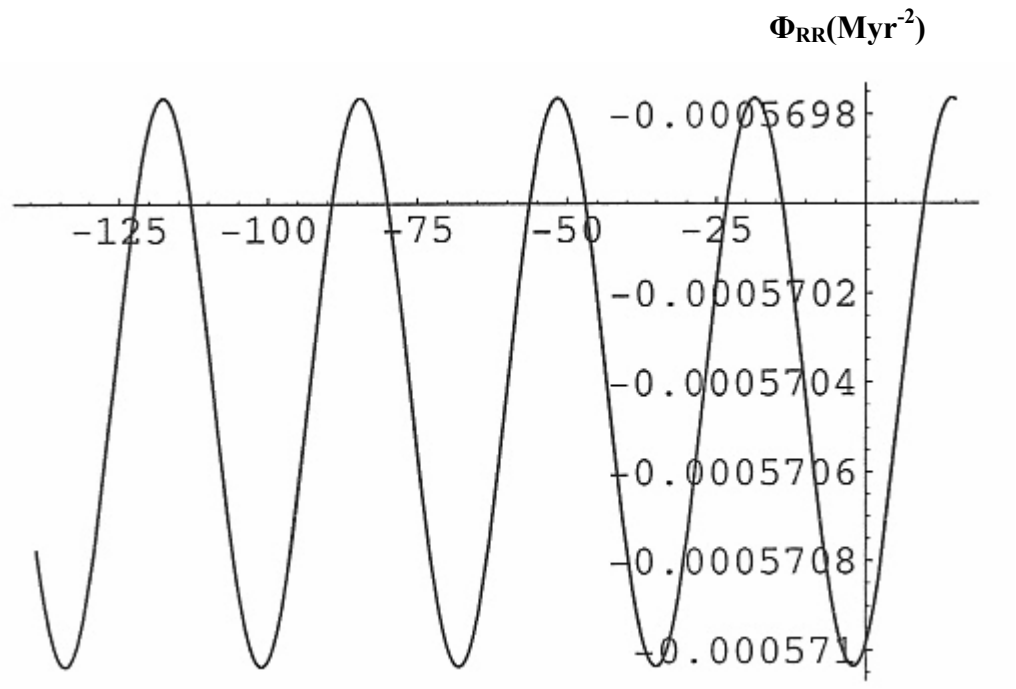

Figure 12: Φ_{RR} as a function of time over the last 139 million years, for our second model orbit with vertical oscillation at constant R.

```
Plot[
 {-0.153 R (0.0768 Sin[2 * Pi (t + 2.1) / 66]) ((R^2 + (0.0768 Sin[2 * Pi (t + 2.1) / 66]) ^2) ^0.5 +
       0.7 (R^2 + (0.0768 Sin[2 * Pi (t + 2.1) / 66]) ^2) ^-0.5 +
       2 (R^2 + (0.0768 Sin[2 * Pi (t + 2.1) / 66]) ^2) ^-1) /
     (0.7 + (R^2 + (0.0768 Sin[2 * Pi (t + 2.1) / 66]) ^2) ^0.5) ^3 -
   3 * 0.450 R (0.0768 Sin[2 * Pi (t + 2.1) / 66])
    (1 + 6.5 ((0.0768 Sin[2 * Pi (t + 2.1) / 66]) ^2 + 0.26 ^2) ^-0.5) /
     (R^2 + (6.5 + ((0.0768 Sin[2 * Pi (t + 2.1) / 66]) ^2 + 0.26 ^2) ^0.5) ^2) ^2.5 - 4 * 0.018 R
    (0.0768 Sin[2 * Pi (t + 2.1) / 66]) / (R^2 + (0.0768 Sin[2 * Pi (t + 2.1) / 66]) ^2 + 12 ^2) ^2,
  -0.00117237 Sin[2 * Pi (t + 2.1) / 66]}, {t, -139, 15}]
```

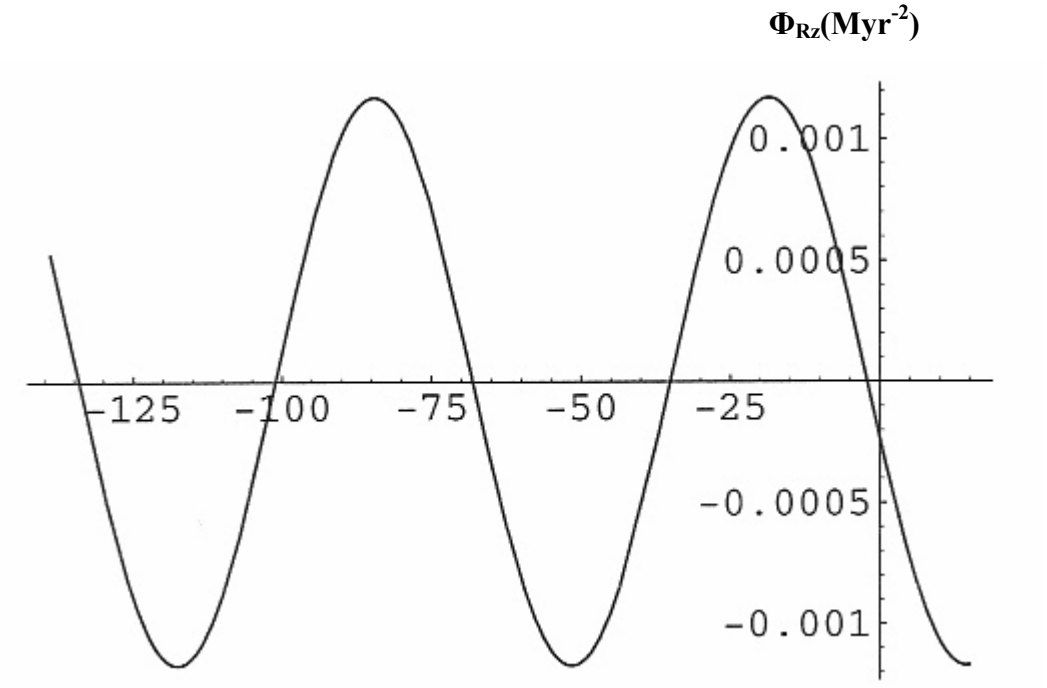

Figure 13: Φ_{Rz} as a function of time over the last 139 million years, for our second model orbit with vertical oscillation at constant R.

```
Plot[{0.153 (1 + 0.7 (9.095^2 + (0.0768 Sin[2 * Pi (t + 2.1) / 66]) ^2) ^-0.5 -
       2 (0.0768 Sin[2 * Pi (t + 2.1) / 66]) ^2 (9.095^2 +
           (0.0768 Sin[2 * Pi (t + 2.1) / 66]) ^2) ^-1 - 0.7 (0.0768 Sin[2 * Pi (t + 2.1) / 66]) ^
         2 (9.095^2 + (0.0768 Sin[2 * Pi (t + 2.1) / 66]) ^2) ^-1.5) /
     (0.7 + (9.095^2 + (0.0768 Sin[2 * Pi (t + 2.1) / 66]) ^2) ^0.5) ^3 -
   3 * 0.450 (0.0768 Sin[2 * Pi (t + 2.1) / 66]) ^2
    (1 + 6.5 ((0.0768 Sin[2 * Pi (t + 2.1) / 66]) ^2 + 0.26^2) ^-0.5) ^2 /
     (9.095^2 + (6.5 + ((0.0768 Sin[2 * Pi (t + 2.1) / 66]) ^2 + 0.26^2) ^0.5) ^2) ^2.5 +
   0.450 (1 + 6.5 ((0.0768 Sin[2 * Pi (t + 2.1) / 66]) ^2 + 0.26^2) ^-0.5 -
       6.5 (0.0768 Sin[2 * Pi (t + 2.1) / 66]) ^2
        ((0.0768 Sin[2 * Pi (t + 2.1) / 66]) ^2 + 0.26^2) - 1.5) /
     (9.095^2 + (6.5 + ((0.0768 Sin[2 * Pi (t + 2.1) / 66]) ^2 + 0.26^2) ^0.5) ^2) ^1.5 +
   2 * 0.018 (9.095^2 - (0.0768 Sin[2 * Pi (t + 2.1) / 66]) ^2 + 12^2) /
     (9.095^2 + (0.0768 Sin[2 * Pi (t + 2.1) / 66]) ^2 + 12^2) ^2,
  0.007731825 + (1.78415 * 10^-4) Cos[2 * Pi (t + 2.1) / 33]}, {t,
  -139,
  15}]
```

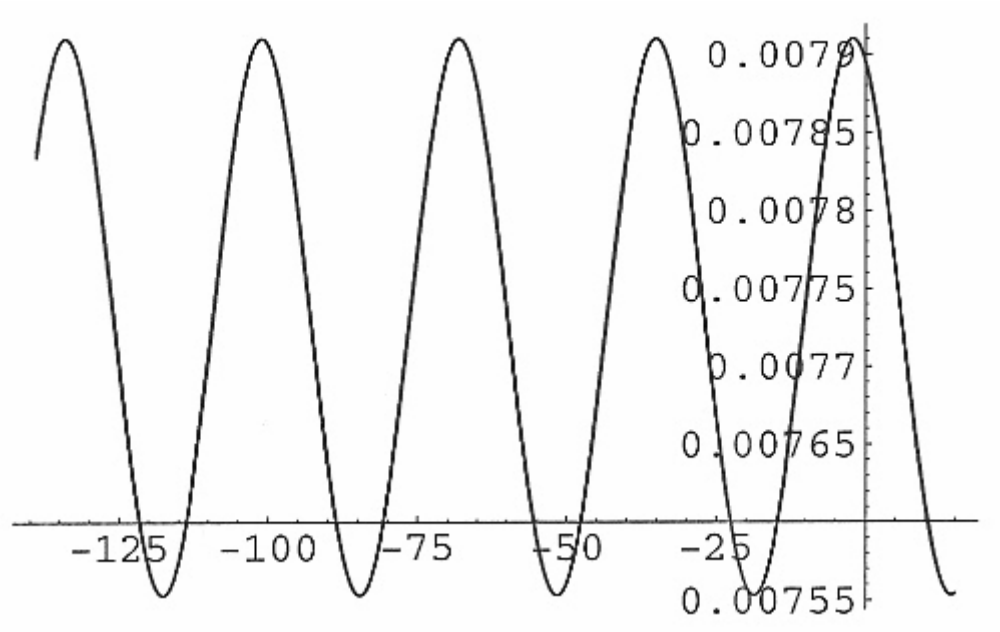

Figure 14: Φ_{zz} as a function of time over the last 139 million years, for our second model orbit with vertical oscillation at constant R.

In Figures 12 & 14 we see a function related to the Sun's vertical oscillation half period of 33 million years, which represents the period of time between successive galactic plane crossings. Again, these complicated functions were fitted with a simpler cosine function using the same method as before. The fit functions are overlayed in the plots shown in Figures 12 to 14 and are expressed by the following equations:

$$\Phi_{RR}(t) = -5.70\times10^{-4}\,\mathrm{Myr}^{-2} - 6.36\times10^{-7}\,\mathrm{Myr}^{-2}\cos(2\pi(t+2.1\mathrm{Myr})/33\mathrm{Myr})$$
$$\Phi_{Rz}(t) = -0.00117\mathrm{Myr}^{-2}\sin(2\pi(t+2.1\mathrm{Myr})/33\mathrm{Myr}) \qquad (14)$$
$$\Phi_{zz}(t) = 0.00773\mathrm{Myr}^{-2} + 1.78\times10^{-4}\,\mathrm{Myr}^{-2}\cos(2\pi(t+2.1\mathrm{Myr})/33\mathrm{Myr})$$

Once again, comparing the strengths of the oscillatory terms suggests that the $\Phi_{zz}(t)$ function, being about 280 times larger in amplitude, dominates over $\Phi_{RR}(t)$. Thus we can conclude that this will have a greater effect on the solar system, and we approximate the overall tidal acceleration with $\delta a_z(t)$. The $\Phi_{Rz}(t)$ function is also large in amplitude but mainly represents a form of tidal shear and not a significant tidal stretching in this case [12].

Model(III)*:* Here both the R(t) and z(t) oscillatory motions of the Sun with respect to the local standard of rest of radius R=9.095 kpc are folded into the expressions for Φ_{RR}, Φ_{Rz} and Φ_{zz}. The time varying second partial derivative functions and their fit functions are plotted in Figures 15,16 & 17.

```
Plot[{0.153
    (1 + 0.7 ((9.095 - 0.6375 Cos[2 * Pi (t - 15) / 154]) ^ 2 + (0.0768 Sin[2 * Pi (t + 2.1) / 66]) ^
            2) ^ -0.5 - 3 (9.095 - 0.6375 Cos[2 * Pi (t - 15) / 154]) ^ 2
        ((9.095 - 0.6375 Cos[2 * Pi (t - 15) / 154]) ^ 2 + (0.0768 Sin[2 * Pi (t + 2.1) / 66]) ^ 2) ^
         -1 - 0.7 (9.095 - 0.6375 Cos[2 * Pi (t - 15) / 154]) ^ 2
        ((9.095 - 0.6375 Cos[2 * Pi (t - 15) / 154]) ^ 2 + (0.0768 Sin[2 * Pi (t + 2.1) / 66]) ^ 2) ^
         -1.5) / (0.7 + ((9.095 - 0.6375 Cos[2 * Pi (t - 15) / 154]) ^ 2 +
           (0.0768 Sin[2 * Pi (t + 2.1) / 66]) ^ 2) ^ 0.5) ^ 3 +
  0.450 (-2 (9.095 - 0.6375 Cos[2 * Pi (t - 15) / 154]) ^ 2 +
      (6.5 + ((0.0768 Sin[2 * Pi (t + 2.1) / 66]) ^ 2 + 0.26 ^ 2) ^ 0.5) ^ 2) /
    ((9.095 - 0.6375 Cos[2 * Pi (t - 15) / 154]) ^ 2 +
      (6.5 + ((0.0768 Sin[2 * Pi (t + 2.1) / 66]) ^ 2 + 0.26 ^ 2) ^ 0.5) ^ 2) ^ 2.5 +
  2 * 0.018 (-(9.095 - 0.6375 Cos[2 * Pi (t - 15) / 154]) ^ 2 +
      (0.0768 Sin[2 * Pi (t + 2.1) / 66]) ^ 2 + 12 ^ 2) /
    ((9.095 - 0.6375 Cos[2 * Pi (t - 15) / 154]) ^ 2 +
      (0.0768 Sin[2 * Pi (t + 2.1) / 66]) ^ 2 + 12 ^ 2) ^ 2,
 -(5.7599 * 10 ^ -4) - (6.0774 * 10 ^ -5) Cos[2 * Pi (t - 15) / 154]},
{t,
 -601,
 15}]
```

$\Phi_{RR}(Myr^{-2})$

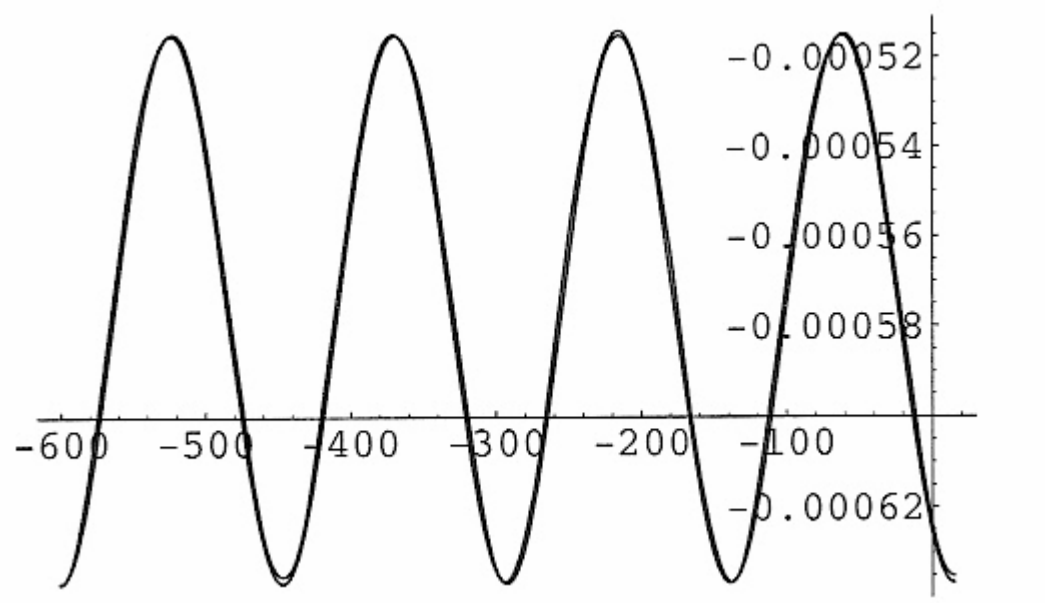

Figure 15: Φ_{RR} as a function of time over the last 601 million years for our model orbit that approximates the solar system's motion.

```
Plot[{-0.153 (9.095 - 0.6375 Cos[2 * Pi (t - 15) / 154]) (0.0768 Sin[2 * Pi (t + 2.1) / 66])
    (((9.095 - 0.6375 Cos[2 * Pi (t - 15) / 154]) ^ 2 + (0.0768 Sin[2 * Pi (t + 2.1) / 66]) ^ 2) ^ 0.5 +
       0.7 ((9.095 - 0.6375 Cos[2 * Pi (t - 15) / 154]) ^ 2 +
            (0.0768 Sin[2 * Pi (t + 2.1) / 66]) ^ 2) ^ -0.5 +
       2 ((9.095 - 0.6375 Cos[2 * Pi (t - 15) / 154]) ^ 2 + (0.0768 Sin[2 * Pi (t + 2.1) / 66]) ^ 2) ^
         -1) / (0.7 + ((9.095 - 0.6375 Cos[2 * Pi (t - 15) / 154]) ^ 2 +
            (0.0768 Sin[2 * Pi (t + 2.1) / 66]) ^ 2) ^ 0.5) ^ 3 -
  3 * 0.450 (9.095 - 0.6375 Cos[2 * Pi (t - 15) / 154]) (0.0768 Sin[2 * Pi (t + 2.1) / 66])
    (1 + 6.5 ((0.0768 Sin[2 * Pi (t + 2.1) / 66]) ^ 2 + 0.26 ^ 2) ^ -0.5) /
     ((9.095 - 0.6375 Cos[2 * Pi (t - 15) / 154]) ^ 2 +
        (6.5 + ((0.0768 Sin[2 * Pi (t + 2.1) / 66]) ^ 2 + 0.26 ^ 2) ^ 0.5) ^ 2) ^ 2.5 -
  4 * 0.018 (9.095 - 0.6375 Cos[2 * Pi (t - 15) / 154]) (0.0768 Sin[2 * Pi (t + 2.1) / 66]) /
    ((9.095 - 0.6375 Cos[2 * Pi (t - 15) / 154]) ^ 2 +
       (0.0768 Sin[2 * Pi (t + 2.1) / 66]) ^ 2 + 12 ^ 2) ^ 2,
 -0.00125051 Sin[2 * Pi (t + 2.1) / 66]}, {t, -601,
 15}]
```

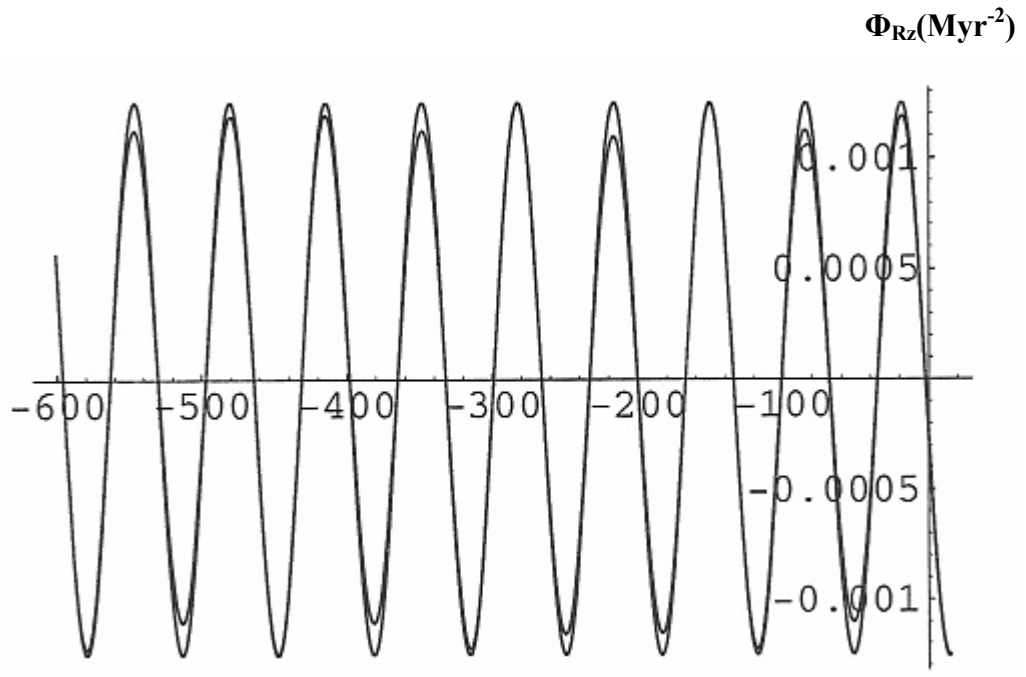

Figure 16: Φ_{Rz} as a function of time over the last 601 million years for our model orbit that approximates the solar system's motion.

```
Plot[{0.153
    (1 + 0.7 ((9.095 - 0.6375 Cos[2 * Pi (t - 15) / 154]) ^ 2 + (0.0768 Sin[2 * Pi (t + 2.1) / 66]) ^
            2) ^ -0.5 - 2 (0.0768 Sin[2 * Pi (t + 2.1) / 66]) ^ 2
        ((9.095 - 0.6375 Cos[2 * Pi (t - 15) / 154]) ^ 2 + (0.0768 Sin[2 * Pi (t + 2.1) / 66]) ^ 2) ^
         -1 - 0.7 (0.0768 Sin[2 * Pi (t + 2.1) / 66]) ^ 2
        ((9.095 - 0.6375 Cos[2 * Pi (t - 15) / 154]) ^ 2 + (0.0768 Sin[2 * Pi (t + 2.1) / 66]) ^ 2) ^
         -1.5) / (0.7 + ((9.095 - 0.6375 Cos[2 * Pi (t - 15) / 154]) ^ 2 +
           (0.0768 Sin[2 * Pi (t + 2.1) / 66]) ^ 2) ^ 0.5) ^ 3 -
   3 * 0.450 (0.0768 Sin[2 * Pi (t + 2.1) / 66]) ^ 2
    (1 + 6.5 ((0.0768 Sin[2 * Pi (t + 2.1) / 66]) ^ 2 + 0.26 ^ 2) ^ -0.5) ^ 2 /
     ((9.095 - 0.6375 Cos[2 * Pi (t - 15) / 154]) ^ 2 +
        (6.5 + ((0.0768 Sin[2 * Pi (t + 2.1) / 66]) ^ 2 + 0.26 ^ 2) ^ 0.5) ^ 2) ^ 2.5 +
   0.450 (1 + 6.5 ((0.0768 Sin[2 * Pi (t + 2.1) / 66]) ^ 2 + 0.26 ^ 2) ^ -0.5 - 6.5
        (0.0768 Sin[2 * Pi (t + 2.1) / 66]) ^ 2 ((0.0768 Sin[2 * Pi (t + 2.1) / 66]) ^ 2 + 0.26 ^ 2) -
       1.5) / ((9.095 - 0.6375 Cos[2 * Pi (t - 15) / 154]) ^ 2 +
        (6.5 + ((0.0768 Sin[2 * Pi (t + 2.1) / 66]) ^ 2 + 0.26 ^ 2) ^ 0.5) ^ 2) ^ 1.5 + 2 * 0.018
    ((9.095 - 0.6375 Cos[2 * Pi (t - 15) / 154]) ^ 2 - (0.0768 Sin[2 * Pi (t + 2.1) / 66]) ^ 2 +
       12 ^ 2) / ((9.095 - 0.6375 Cos[2 * Pi (t - 15) / 154]) ^ 2 +
        (0.0768 Sin[2 * Pi (t + 2.1) / 66]) ^ 2 + 12 ^ 2) ^ 2,
  0.001137105 Cos[2 * Pi (t - 15) / 154] + 0.007731825 +
   (1.78415 * 10 ^ -4)
    Cos[2 * Pi (t + 2.1) / 33]}, {t, -601, 15}]
```

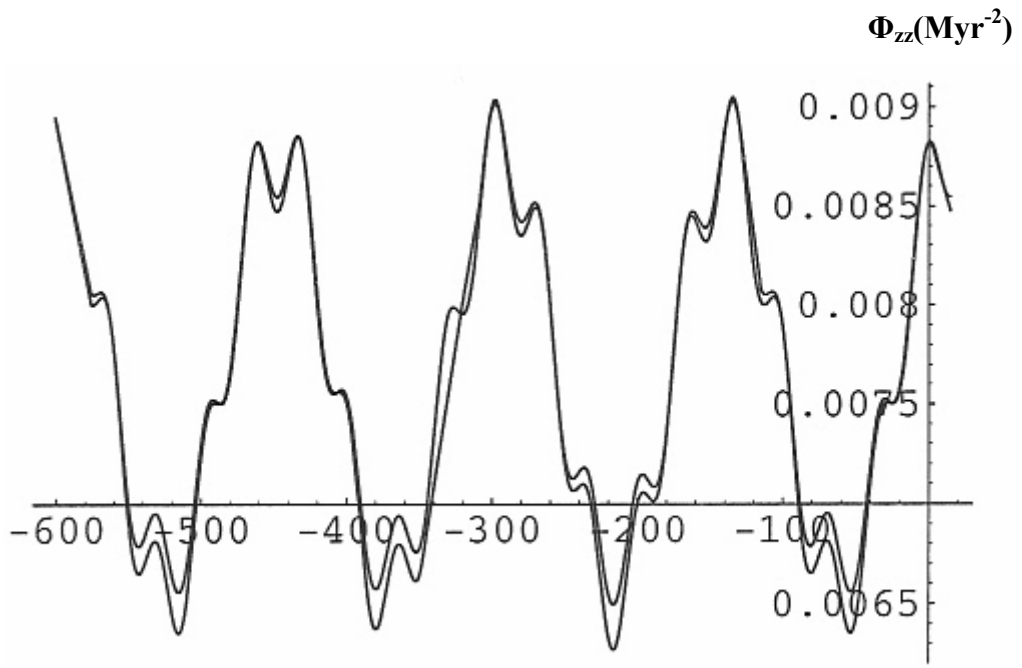

Figure 17: Φ_{zz} as a function of time over the last 601 million years for our model orbit that approximates the solar system's motion.

The fit functions in these plots are simply the sums of the fit functions for the first two models. The fact that the sum of the fit functions from Model(I) and Model(II) matches quite closely the actual $\Phi_{zz}(t)$ function of Model(III) suggests that this component of the galactic tidal field can be modelled reasonably well by a linear combination of the fit functions from the first two model orbits. The $\Phi_{zz}(t)$ function dominated over $\Phi_{RR}(t)$ for both of these cases, and so we use the last $\Phi_{zz}(t)$ function to

get a reasonable approximation of the overall tidal acceleration function for the solar system's motion in the galaxy over time.

Calculation of Magnitudes of Tidal Deformation

Many physicists dismiss galactic tidal influences on the solar system as negligible due to the magnitudes involved. If we compare the gravitational field at the Earth's orbit due to the Sun, approximately 5.93×10^{-3} ms^{-2}, to the gravitational field at the solar system's current position due to the galaxy, 3.33×10^{-10} ms^{-2}, the effect of the galaxy seems miniscule. The zz component of the galactic tidal field at the solar system's current position has a magnitude of 8.07×10^{-30} s^{-2}, which is incredibly slow by the standard that scientists are used to dealing with. However, galactic tidal forces should not be negated entirely due to the enormous timescales on which galactic tidal forces exert their influence. Having determined how the galactic tidal forces act on the solar system over time, we can now get a rough estimate for the magnitude of the change in the Earth-Sun distance. This calculation is performed using the assumption that the solar system behaves like a system of free particles with no interaction between the particles in the system. An example of this would be a ball of dust floating in space. As opposed to treating the solar system like a system of bound particles to which it most definitely is. Nonetheless, we need to follow this assumption here to make the calculation possible and we will describe the limitations resulting from this assumption after the calculation.

So we will calculate a tidal deformation from the largest contributing components, the $\Phi_{zz}(t)$ terms, of our first two model star orbits. Because the Φ_{zz} results from Model(III) can be approximated by a linear combination of Models (I) and (II), we can study the overall tidal deformation by looking at the Model(I) and Model(II) contributions individually. And so for the first case, we can estimate the tidal deformation in the z direction for the radially oscillating orbit of Model(I) from the presently approaching tidal maximum, 15 Myr into the future, to the last tidal minimum, approximately 62 Myr in the past, by subtracting the mean term from $\Phi_{zz}(t)$ and integrating the oscillatory term twice with respect to time. The first integration transforms the acceleration into a speed, and the second transforms the speed into a distance.

$$\delta z = \sin\ i \times 1\ \text{AU} \int_{+15}^{-62} \int_{+15}^{-62} \Phi_{zz}(t)(dt)^2$$
$$= 0.868\ \text{AU} \int_{+15}^{-62} \int_{+15}^{-62} [0.00846\text{Myr}^{-2} + 0.00114\text{Myr}^{-2} \cos(2\pi(t - 15\text{Myr})/154\text{Myr})](dt)^2$$

To make the integration easier without changing the total value of the integral, we decide to change the phase with the substitution $\tau = t - 15$.

$$\delta z = 0.868\ \text{AU} \int_{0}^{-77} \int_{0}^{-77} 0.00114\text{Myr}^{-2} \cos(2\pi\tau/154\text{Myr})(d\tau)^2$$
$$= 0.868\ \text{AU} \times -0.00114(154/2\pi)^2 \left[\cos(2\pi\tau/154\text{Myr})\right]_0^{-77} = 1.19\ \text{AU} \quad (15)$$

In the second integration we evaluate the tidal deformation from the last local tidal maximum, approximately 2.1 Myr ago, to the last local tidal minimum, approximately 18.6 Myr ago, with the tidal field function from the second model orbit.

$$\delta z = \sin\ i \times 1\ \text{AU} \int_{-2.1}^{-18.6} \int_{-2.1}^{-18.6} \Phi_{zz}(t)(dt)^2$$
$$= 0.868\ \text{AU} \int_{-2.1}^{-18.6} \int_{-2.1}^{-18.6} [0.00766\text{Myr}^{-2} + 2.51 \times 10^{-4}\text{Myr}^{-2} \cos(2\pi(t + 2.1\text{Myr})/33\text{Myr})](dt)^2$$

Here we change the phase of the integral with the substitution $\tau = t + 2.1$.

$$\delta z = 0.868\ \text{AU} \int_{0}^{-16.5} \int_{0}^{-16.5} 2.51 \times 10^{-4}\text{Myr}^{-2} \cos(2\pi\tau/33\text{Myr})](d\tau)^2$$
$$= 0.868\ \text{AU} \times -2.51 \times 10^{-4}(33/2\pi)^2 \left[\cos(2\pi\tau/33\text{Myr})\right]_0^{-16.5} = 0.0120\ \text{AU} \quad (16)$$

The constant terms, 0.00846Myr^{-2} and 0.00766Myr^{-2}, need to be left out of the integration because otherwise this would treat the solar system as if it were in free fall, to which it is not. We integrate the cosine terms by themselves and thus measure the tidal deformation using the Sun's oscillatory motion alone.

The results we arrive at are 1.19 AU and 0.0120 AU. However, in the first case, since the tidal deformation is greater than the astronomical unit this means that the Earth would have been closer to the Sun than the planet Venus is today. This is impossible given what the evidence from the geological record suggests. Undoubtedly, the unrealistic results seen in these calculations are a consequence of treating the solar system as a ball of dust with no interaction between the particles in the system. Nonetheless, we have shown that the solar system is immersed within the galactic tidal field, and the magnitude of the resulting change to the Earth-Sun distance on large timescales remains to be calculated rigorously.

Discussion of Uncertainties and Assumptions

To make the calculations in this report possible, the model we used for the galactic potential was also simplified by neglecting θ dependent phenomena like spiral arms. This was necessary in this preliminary model because θ dependent potentials greatly increase in complexity and can no longer be described using analytic functions. Adding θ dependence into the potential is also difficult due to the uncertainty and lack of understanding about galactic spiral structure. Some commonly used θ-dependent potentials are discussed in graduate-level texts.

It is also quite evident that i, the inclination angle is bound to change over time because of the differential influence of the tides in different directions. Therefore this calculation loses its accuracy as the timescale increases and the solar system changes its orientation in the galaxy. Not to mention the fact that the solar system actually has a three-dimensional representation in galactic coordinates and the galactic center is not far in the sky from the intersection of the plane of the Milky Way and the ecliptic. This means that for the triangle representing the orientation of the solar system shown in Figure 4, the triangle should actually be pointed mainly in the $\Delta\theta$ direction instead of the ΔR direction. We didn't take this three-dimensional approach in the calculation because it would have to involve bringing θ dependence into the potential. However, it is important to mention that this does not change the current value for Δz, which is derived directly from the North Galactic Pole's ecliptic latitude, and is the component of the solar system most affected by galactic tidal forces in the models we used.

Conclusion

The question of whether or not galactic tidal perturbations affect the solar system to any noticeable degree will have to rest upon further research using more thorough calculations. In this case, future models of the solar system's motion in the galaxy should also account for θ dependent phenomena like the spiral arms of the galaxy, which although more complex, will help to provide a more accurate estimate of the local galactic tidal field and its influence on the solar system. The other variable that future research in this field will undoubtedly have to account for is the interaction between bodies in the solar system. This will provide a better estimate for the magnitudes of

galactic tidal influences on the solar system, at the risk of making the calculations slightly more complex.

However, if galactic tidal forces have a significant influence on orbits in the solar system, this may have implications for comet activity, climate, and consequently the evolution of life on earth and other planets. In this case, it may even be possible to use the geological record to learn information about our galaxy that we cannot see with our eyes and our telescopes. Our spaceship, the Earth, has been travelling through the cosmos for much longer than we as humans have been able to make detailed astronomical observations of our galaxy. Over the enormous timeframe of geological history, the geological record has acted like a flight recorder for the spaceship, preserving vital information about our planet's journey through the Milky Way. In this case, the geological record is a vast and invaluable resource, a tape that has been running for millions and billions of years that may shed light on things that have so far been hidden from view.

Acknowledgements

I would like to thank, first and foremost, my supervisor Dr. Langill for agreeing to overlook the project. I would also like to thank Dr. Stil, Dr. Hobill and Dr. Ouyed for their kind assistance over the course of the semester. And of course, all the friends I've met in school and in other places.

Appendix

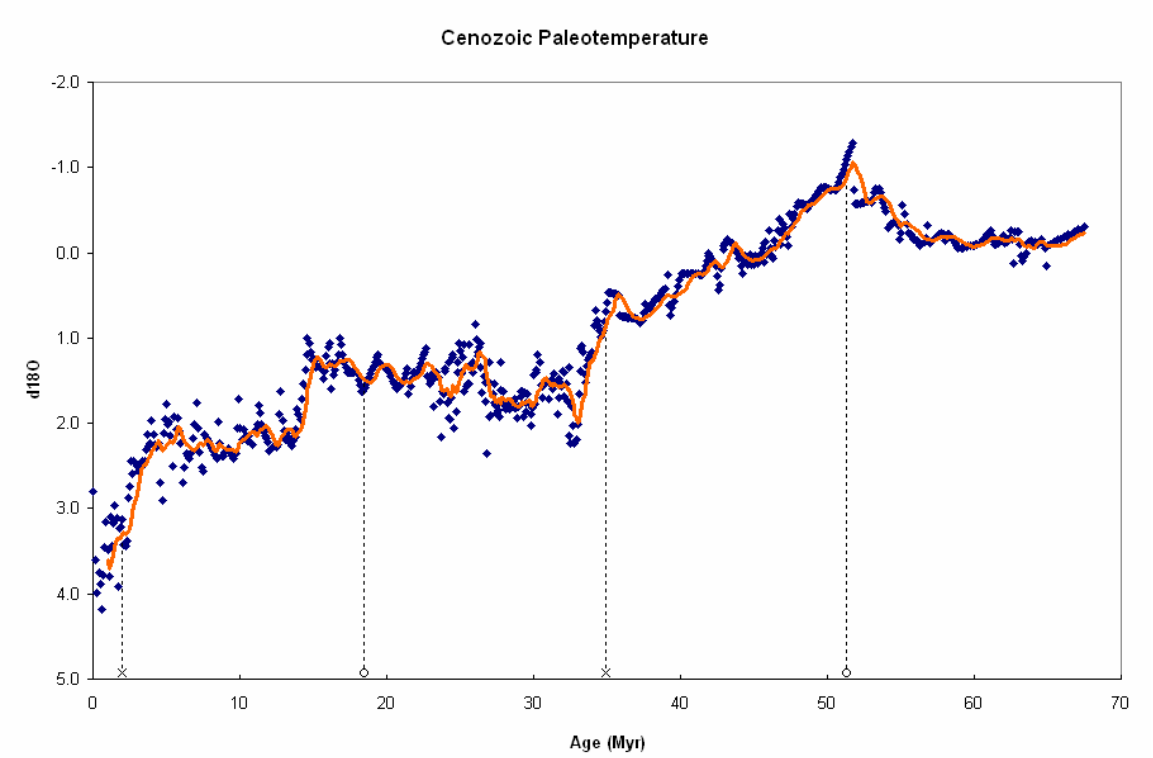

Figure 18: The last 70 million years of global climate, palaeotemperature data derived from oxygen isotope analysis of benthic foramnifera. Data from Miller et al. 1987[9], using 680 measurements and then applying a 10 Myr moving average to the sample. The X's denote times of galactic plane crossings (local tidal maxima) and O's denote times of maximum vertical heights above and below the galactic plane (local tidal minima) as defined by F. Bash, 1986.

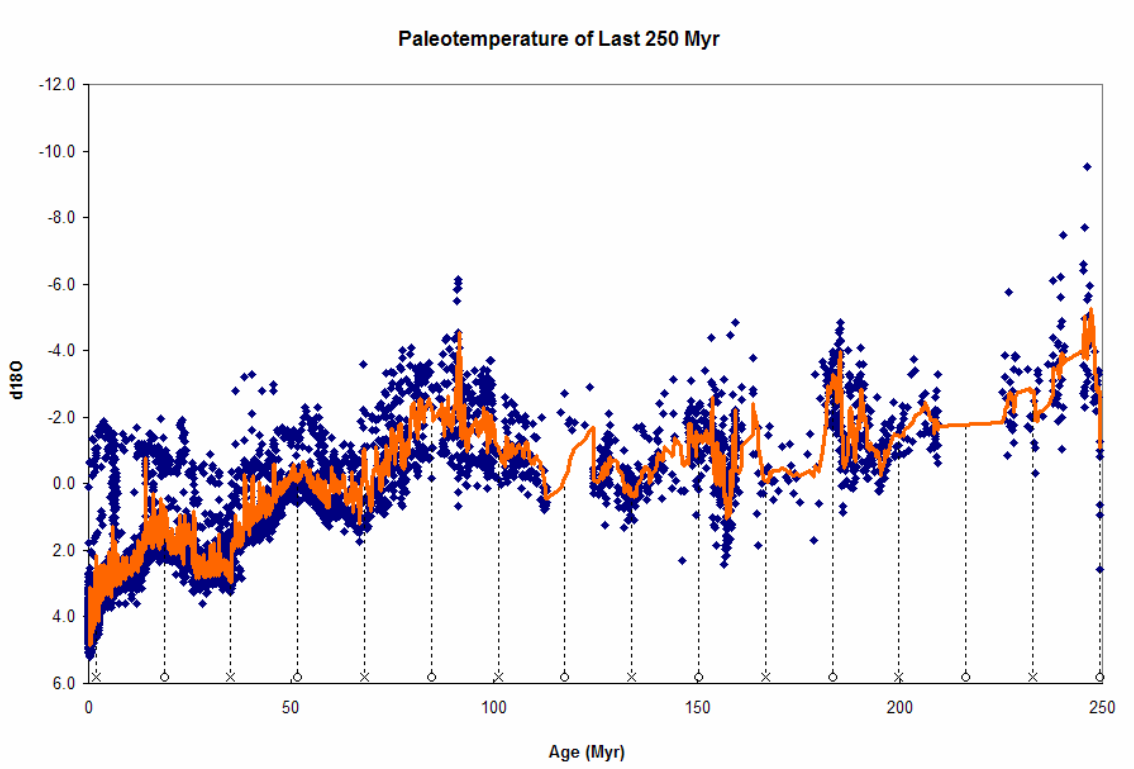

Figure 19: Paleotemperature over the last 250 million years estimated from oxygen isotope analysis of fossils. Data is from Veizer et al, 2004[10] using over 13,000 measurements of a variety of fossil organisms, and then applying a 10 Myr moving average to the sample. The X's denote times of galactic plane crossings (local tidal maxima) and O's denote times of maximum vertical heights above and below the galactic plane (local tidal minima) as defined by F. Bash, 1986. Could this be related to the Solar System's motion in the Galaxy?

References

[1]Bash F., "The Present, Past and Future Velocity of Nearby Stars: The Path of the Sun in 10^8 Years." In The Galaxy and the Solar System, ed. Smoluchowshi R., Bachall J.N., Matthews M.S., (1986): 35-46.

[2]Binney J., Merrifield M., "Galactic Astronomy." Princeton University Press, Princeton (1998).

[3]Binney J., Tremaine S., "Galactic Dynamics." Princeton University Press, Princeton (1987).

[4]Flower B.P., "Cenozoic Deep-Sea Temperatures and Polar Glaciation: The Oxygen Isotope Record." Terra Antarctica Reports, 3 (1999): 27-42.

[5]Flynn C., Sommer-Larsen J., Christensen P.R., "Kinematics of the Outer Stellar Halo." RAS, MNRAS, 281(3), (1996): 1027-1032.

[6]Grillmair C., Johnson R., "The Detection of a 45° Tidal Stream Associated with the Globular Cluster NGC 5466." Astrophys. J., 639(1), (2006): L17-L20.

[7]Helmi A., White S.D.M., "Simple dynamical models of the Sagittarius dwarf galaxy." RAS, MNRAS, 323 (2001): 529-536.

[8]Jones M.H., Lambourne R.J.A., "An Introduction to Galaxies and Cosmology." Cambridge University Press, Cambridge (2004).

[9]Miller K.G., Fairbanks R.G., Mountain G.S., "Tertiary Oxygen Isotope Synthesis, Sea Level History, and Continental Margin Erosion." Paleoceanography, 2(1), (1987): 1-19.

[10]Veizer J., et al, Online database: http://www.science.uottawa.ca/geology/isotope_data/ (2004).

[11]Zeilik M., Gregory S., "Introductory Astronomy & Astrophysics, 4th Edition." Saunders College Publishing, Philadelphia (1998).

[12]Personal communication with Dr. David Hobill, Department of Physics & Astronomy, University of Calgary.